

Electrochemical Characterization of Submicron Size Particles of LiMn_2O_4 in Aqueous Electrolytes

Nupur Nikkan Sinha¹, P. Ragupathy², H.N. Vasan² and N. Munichandraiah^{1,*}

¹ Department of Inorganic and Physical Chemistry; Indian Institute of Science, Bangalore - 560 012, India

² Solid State and Structural Chemistry Unit; Indian Institute of Science, Bangalore - 560 012, India

*E-mail: muni@ipc.iisc.ernet.in

Received: 9 February 2008 / Accepted: 25 March 2008 / Online published: 20 April 2008

Spinel LiMn_2O_4 is synthesized by inverse microemulsion route and particles of size less than 200 nm are obtained. The electrochemical characterization of the sub-micron size particles of LiMn_2O_4 is carried out in an aqueous solution of 5 M LiNO_3 . In cyclic voltammetry, LiMn_2O_4 electrodes exhibit two pairs of reversible redox peaks and accordingly separate potential plateaus are observed during charge-discharge cycling. Electrochemical impedance data measured at various temperatures and various state-of-charge (SOC) values are analyzed to calculate exchange current, activation energy and transfer coefficient for $\text{Mn}^{4+}/\text{Mn}^{3+}$ redox process in LiMn_2O_4 , which accompanies intercalation/deintercalation of Li^+ ions. Impedance data are subjected to non-linear least squares fit procedure using an appropriate electrical equivalent circuit and charge-transfer resistance (R_{ct}) of the redox process is evaluated. The kinetic parameters of the process are calculated from variations of R_{ct} with temperature and SOC of LiMn_2O_4 electrode in 5 M LiNO_3 aqueous electrolyte. A typical cell employing LiMn_2O_4 as the positive electrode and V_2O_5 as the negative electrode was assembled and characterized by charge-discharge cycling in 5 M LiNO_3 aqueous electrolyte.

Keywords: LiMn_2O_4 ; sub-micron size particles; microemulsion route; aqueous electrolyte.

1. INTRODUCTION

During the past two decades, intense research activities on the Li-ion battery active materials have been in progress [1,2]. As it is constructed on the basis of two electrode materials, whose potential values differ widely in non-aqueous electrolytes, the cell voltage of Li-ion system is as high as 3.5 V. This high value of cell voltage essentially contributes to realize a high value of energy density (both gravimetric and volumetric). Typically, LiCoO_2 and lithiated carbon are used as the positive and negative electrodes, respectively. In both these materials, Li^+ ions can undergo

electrochemical intercalation/deintercalation during the charge-discharge cycling. During the charging process, Li^+ ions are deintercalated from the positive electrode into the electrolyte, and simultaneously they get intercalated into the negative electrode from the electrolyte. The reverse reactions take place during the discharge process. Thus, the mechanism of Li-ion cells is known as shuttle-cock mechanism. The cell can be subjected to charge-discharge cycling between 3.0 and 4.2 V. The electrochemistry of these Li-ion cells in non-aqueous electrolytes is different from that of conventional batteries such as Pb-acid, Ni-Cd, etc., which are based on aqueous electrolytes [3]. In aqueous electrolytes the positive and negative electrodes are chosen in such a way that the electrolysis of water does not take place during charge-discharge cycling of the cell.

It was shown by Li et al., that intercalation/deintercalation of Li^+ ions into/from some lithium transition metal oxides such as LiMn_2O_4 can take place in aqueous electrolytes of Li salts also [4]. The potentials of these electrode materials fall between the potentials of oxygen and hydrogen electrodes in the electromotive force series. Using LiMn_2O_4 and V_2O_5 for positive and negative electrodes, respectively, coin cells in 5 M aqueous LiNO_3 solution were assembled. The cell reaction in aqueous electrolytes is also the same as in the non-aqueous Li-ion cells, namely, shuttling of Li^+ ions between positive and negative electrodes during charge-discharge cycling. The cell showed an excellent reversibility with an average voltage of about 1.5 V. This value of cell voltage is considerable lower than the non-aqueous Li-ion cells, which leads to a decreased energy density. Nevertheless, the advantages anticipated from aqueous Li-ion cells are ease of cell assembly, low cost, high safety and environmental friendliness. In particular, the risk associated with poor thermal stability of Li-ion cells in non-aqueous electrolytes is a serious problem. Frequent incidents of burning and explosion of these cells as well as the equipment are sources for a serious concern for common users as well as for scientists and technologists.

Particle size of the electrode materials employed for battery electrodes play an important role in battery performance. In order to realize high rate capabilities of the cells, it is necessary to employ the electrode active materials with smaller particles. With smaller particle size, diffusion path-length is smaller and therefore the rate of electrochemical process is greater, which enhances the rate capability of the electrode. If nano particles are used for enhancing the rate capability, a high reactivity of these particles with the electrolyte leads to poor cycling performance of the cells. Thus on one hand, micron size particles lead to poor rate capability with a long cycle life, and on the other hand, nano size particles lead to high rate capability with poor cycle-life. The desirable particle size, therefore, should be in between micrometer and nanometer ranges. In this context, sub-micron size particles of electrode materials are important.

There are no studies reported in literature on synthesis of sub-micron size particles of LiMn_2O_4 and characterization in aqueous Li salts, to the best of authors' knowledge. Also, studies on basic electrochemical properties such as exchange current, transfer coefficient, activation energy, etc., of the $\text{Mn}^{3+}/\text{Mn}^{4+}$ redox reaction occurring in LiMn_2O_4 during intercalation/deintercalation of Li^+ ions are scarce, although studies on synthesis, physical characterization, structural characterization and battery related investigations in non-aqueous electrolytes are plentiful. Focusing on sub-micron size particles and electrochemical properties, in the present study, LiMn_2O_4 particles are prepared by inverse microemulsion route and properties of the redox reaction in aqueous LiNO_3 electrolyte are investigated

by electrochemical impedance spectroscopy. Also, LiMn_2O_4 prepared is found to possess high rate capability.

2. EXPERIMENTAL PART

Analytical grade reagents, namely, lithium acetate (Aldrich), manganese acetate (Spectrochem), cyclohexane (Merck), high purity sodium dodecyl sulfate (SDS, Merck) and n-butanol (SD Fine Chemicals) were used for the experiments. Solutions were prepared in doubly distilled water. LiMn_2O_4 was synthesized in quaternary micro emulsion medium, which consisted of water, cyclohexane, SDS and n-butanol. A solution was prepared by mixing 51.2 ml cyclohexane (oil), 6.2 ml of n-butanol (co-surfactant), and 0.225 g of SDS (surfactant) and stirred well until it became optically transparent. To this non-aqueous medium, 10 ml aqueous solution of 1 M $\text{Mn}(\text{CH}_3\text{COO})_2$ and 10 ml aqueous solution 0.5 M CH_3COOLi were added. The emulsion medium was stirred for 12 h at ambient conditions followed by evaporation at 120 °C to obtain a brown gel. The gel was heated at 400 °C in air for 6 h and a precursor was obtained. The quantity of the precursor obtained in a batch of synthesis was about 0.450 g. Subsequently, the precursor was heated at different temperatures ranging from 500 to 900 °C for 6 h to get dry powders. V_2O_5 was prepared by polyol route. Details of synthesis and characterization of V_2O_5 will appear elsewhere [5]. This compound was used for a few studies in combination with LiMn_2O_4 prepared in the present work.

For electrochemical characterization, electrodes were prepared on stainless steel (SS, 0.2 mm thick) as a current collector. The SS foil was sandblasted to remove the surface oxide layer and to generate a rough surface. A foil of 1 cm² area with a tag for electrical connection was etched in dil. HNO_3 , cleaned with detergent, washed with doubly distilled water, rinsed with acetone, dried and weighed. LiMn_2O_4 (70 wt %), acetylene black (25 wt %) and polyvinylidene fluoride (5 wt %) were ground in a mortar; a few drops of 1-methyl-2-pyrrolidinone were added to get a syrup. It was coated on to the pretreated SS-foil (area 1 cm²) and dried. Coating and drying steps were repeated to get the required loading level (4-6 mg) of the active material. Finally the electrodes were dried at 110 °C under vacuum for 12 h. V_2O_5 electrodes were also prepared in a similar procedure. The electrochemical values per unit mass are reported on the basis of active material mass. The electrochemical cells were assembled in a glass cell of 25 ml capacity using 5 M LiNO_3 aqueous solution as the electrolyte, Pt foils as the counter electrodes and a saturated calomel electrode (SCE) as the reference electrode. All potential values are reported against SCE. For conducting the pH dependent experiments, dil. HNO_3 or dil. LiOH was added to 5 M LiNO_3 solution to reach the desired pH value. $\text{V}_2\text{O}_5 - \text{LiMn}_2\text{O}_4$ cells were assembled in 5 M LiNO_3 solution of pH 6.5.

Powder X-ray diffraction (XRD) patterns of the samples were recorded using a Philips XRD X'PERT PRO diffractometer with $\text{CuK}\alpha$ ($\lambda = 1.5418 \text{ \AA}$) as the source. Microstructures were examined by FEI-scanning electron microscope model SIRION and FEI-high resolution transmission electron microscope (HRTEM) model TECNAI F30. Chemical analysis of the samples was carried out using Varian inductively coupled plasma atomic emission spectrometer model Vista-PRO. Cyclic voltammograms were recorded with an EG&G potentiostat model Versastat. The impedance spectra

were recorded potentiostatically at open circuit potential with an ac excitation signal of 5 mV (peak to peak) over the frequency range from 100 kHz to 0.01 Hz using Solartron potentiostat/galvanostat model 1287 in combination with Solartron frequency response analyzer model 1250. Impedance data were subjected to non-linear least squares (NLLS) fitting procedure. Constant current charge-discharge cycling of the electrodes was performed using Solartron potentiostat/galvanostat model 1287. For conducting experiment in the temperature range from -5 to 40 °C, a Julabo refrigerator-cum heater Model F25, with ethanol as the thermal medium, was employed. At each desired temperature, the cell was equilibrated for 3 h before conducting the measurements. The ambient temperature experiments were carried out at 20 ± 1 °C in an air conditioned room.

3. RESULTS AND DISCUSSION

3.1. Synthesis

In the inverse micro emulsion route, the reactants are allowed to combine in micrometer or sub-micrometer size drops of aqueous phase, which are dispersed in a large volume of organic phase [6]. The aqueous droplets are stabilized by surfactant molecules, which are oriented in the form of reverse micelles. As the growth of the reaction product is limited by the size of the aqueous droplets in these nanoreactors, the particle size obtained is in sub-micrometer or nanometer scale. In the present synthesis, inter mixing of the reactants took place within the aqueous droplets. Slow evaporation of the emulsion resulted in the formation of a gel consisting of acetates of Mn and Li in narrow regions, which were surrounded by surfactant molecules. During the subsequent heat treatment, the mixed metal acetates as well as the surfactant were oxidized resulting in the formation of sub-micron size particles of LiMn_2O_4 .

3.2. The effect of temperature

Thermal analysis of the precursor sample is shown in Fig. 1(A). In the thermo-gravimetric analysis (TGA) curve, there is about 2.5 % weight loss when the sample is heated up to 200 °C, which is due to adsorbed water. There is about 5.5 % weight loss between 200 and 350 °C due to the removal of acetates, which is followed by 2 % weight loss due to the removal of surfactant molecules. The two exothermic peaks observed in differential thermal analysis (DTA) curve at 130 and 820 °C, respectively, are attributed to the removal of organic parts of the reactants and sodium of the SDS molecules. The emulsion derived precursor was heated at different temperatures between 400 and 900 °C. The XRD patterns of the samples heated at 800 and 900 °C are shown in Fig. 1(B). It is known that LiMn_2O_4 crystallizes in cubic spinel structure with the space group $Fd\bar{3}m$. The XRD patterns of the samples obtained at 800 and 900 °C (Fig. 1(B)) agree with the pattern of pure cubic spinel phase of LiMn_2O_4 (JCPDS file No. 35-782). The intensity ratio of (111) and (311) (or (400)) peaks is high. The values of lattice parameter $a = 8.201$ and 8.239 Å, respectively, obtained for the samples heated at 800 and 900 °C agree well with the values reported in the literature [7]. For the samples heated below 800 °C, some impurity peaks were observed. Chemical analysis of the sample obtained at 900 °C revealed

that a small amount (about 2 wt %) of sodium was present as an impurity, which originated from SDS surfactant. Nevertheless, the electrochemical performance of this sample was not affected by sodium initially present in the compound, as detailed below.

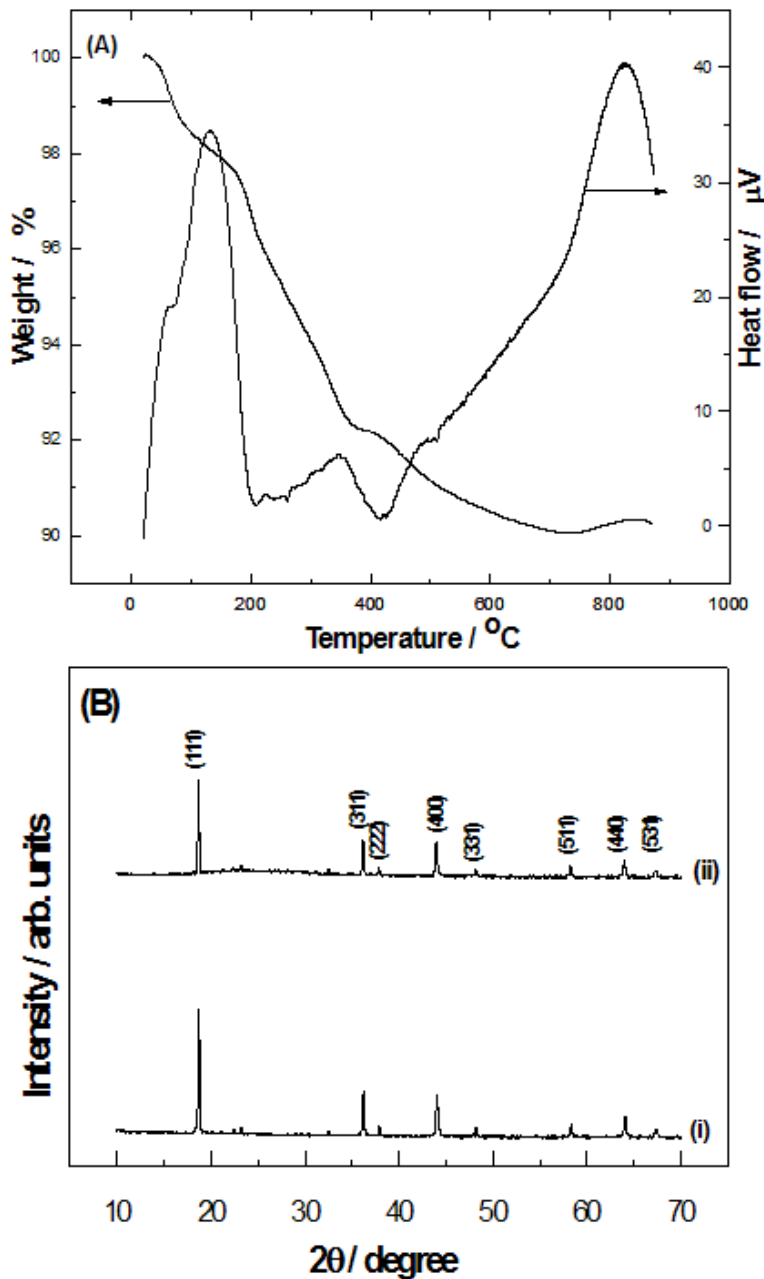


Figure 1. (A) TGA (i) and DTA (ii) curves of precursor LiMn_2O_4 recorded at a heating rate of $10\text{ }^\circ\text{C min}^{-1}$, and (B) powder XRD patterns of LiMn_2O_4 samples obtained by heating the precursor at temperature $800\text{ }^\circ\text{C}$ (i) and $900\text{ }^\circ\text{C}$ (ii).

SEM, TEM and HRTEM micrographs of LiMn_2O_4 samples heated at $900\text{ }^\circ\text{C}$ are shown in Fig. 2. The particles are non-spherical in shape with an average size of about 200 nm (Fig. 2A). TEM image

also confirms cubic or hexagonal shaped particles of about or less than 200 nm (Fig. 2B). HRTEM micrograph (Fig. 2C) exhibits clear lattice fringes with a separation of 4.759 Å. This value corresponds to (111) plane of the cubic lattice of LiMn_2O_4 .

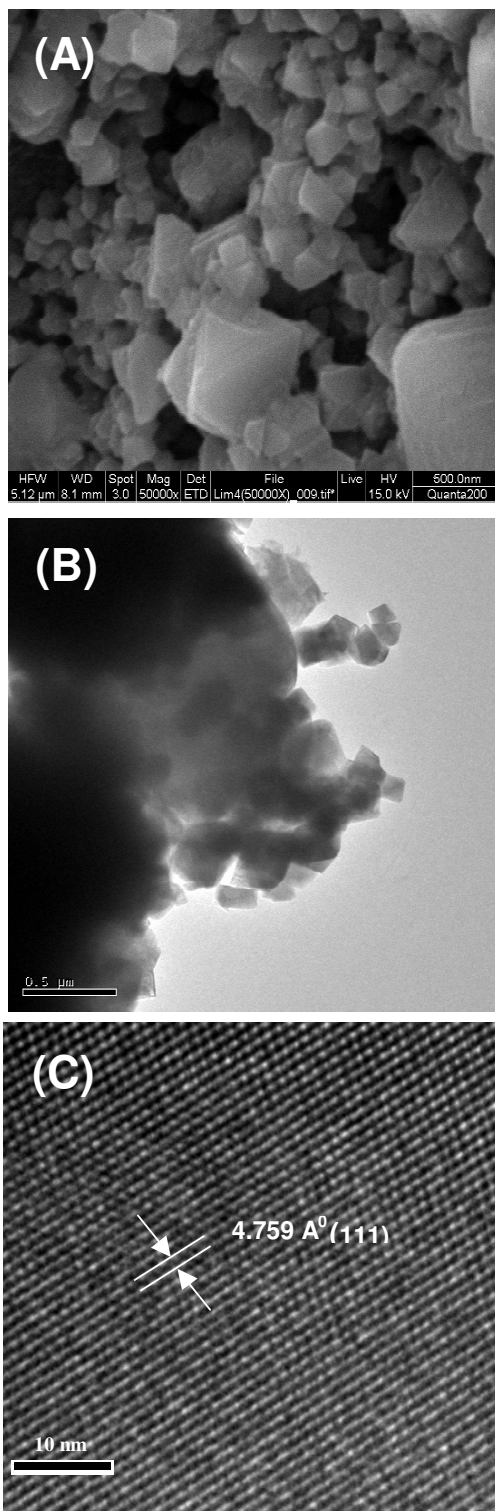


Figure 2. (A) SEM and (B) TEM and (C) HRTEM images of LiMn_2O_4 powder prepared at 900 °C.

3.3. Cyclic voltammetry in aqueous media

Cyclic voltammograms of a LiMn_2O_4 electrode recorded at various sweep rates in 5 M LiNO_3 electrolytes of different pH values are shown in Fig. 3. In all electrolytes, two pairs of redox peaks are clearly observed at low sweep rates. The anodic current peaks are, typically at 0.2 mV s^{-1} , centered at 0.84 and 0.97 V, while the corresponding cathodic peaks at 0.83 and 0.96 V. In general, the peak currents of the first pair of redox peaks are found to be smaller than the second pair of redox peaks in

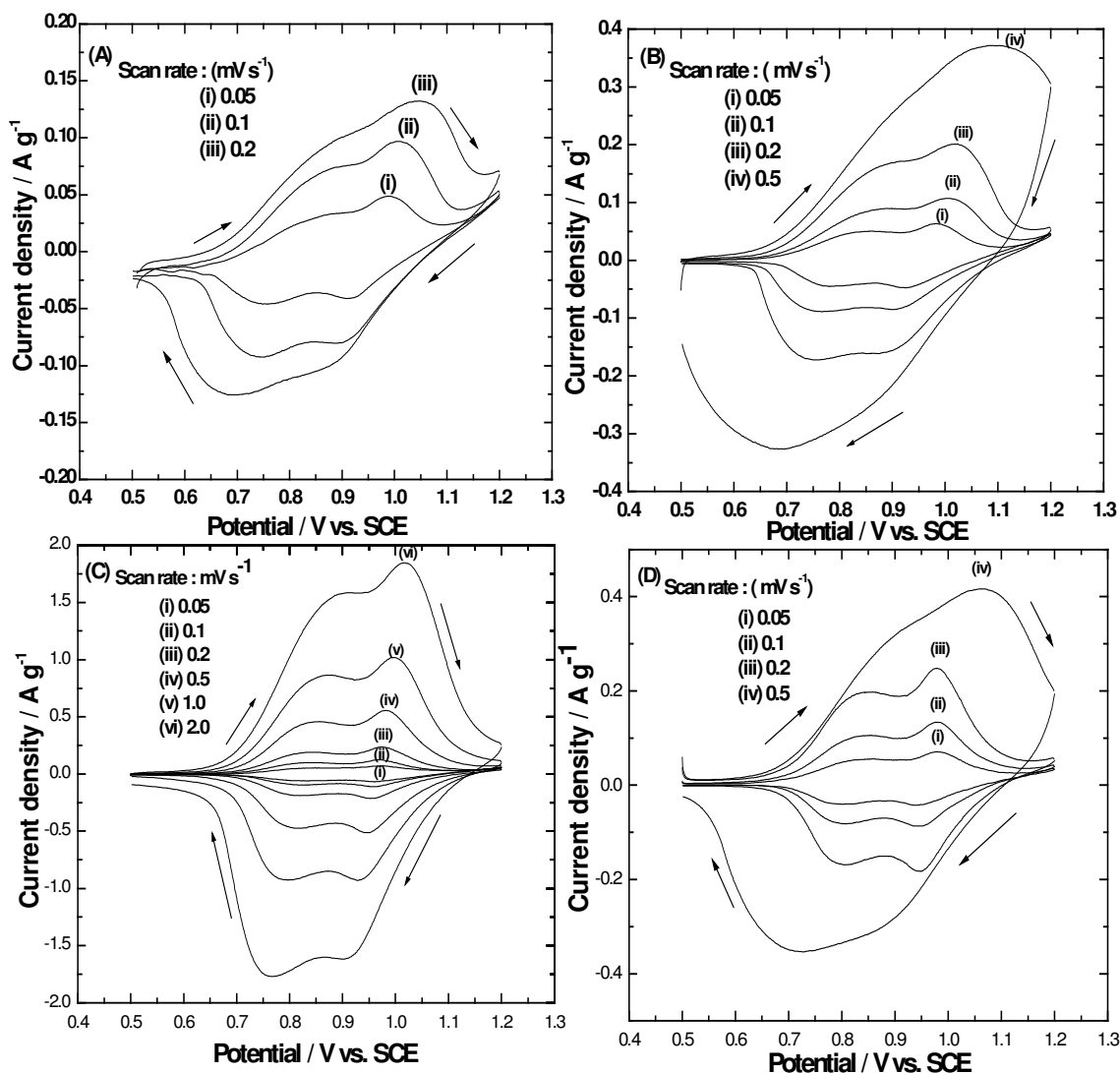


Figure 3. Cyclic voltammograms of LiMn_2O_4 electrode in 5 M LiNO_3 aqueous electrolytes of pH (A) 1.5, (B) 4.2, (C) 6.5, and (D) 9.5.

all electrolytes. Cvjeticanin et al., have recently compared the cyclic voltammetric behavior of LiMn_2O_4 and $\text{LiCr}_{0.15}\text{Mn}_{0.85}\text{O}_4$ in aqueous LiNO_3 electrolyte [8]. In the case of LiMn_2O_4 , the heights of the second redox peaks were greater than the heights of the first pair of redox peaks, where as it was

opposite in the case of Cr substituted sample. Increased height of the second pair of redox peaks in voltammogram of LiMn_2O_4 , similar to the present study, was expected to provide higher charge/discharge capacity in high potential region. The appearance of two pairs of redox peaks in aqueous electrolytes (Fig. 3) is similar to the behavior of LiMn_2O_4 in non-aqueous electrolytes [9]. On charging of the electrode, Li^+ ions are removed from two different lattice sites in LiMn_2O_4 , and this leads to appearance of two anodic peaks. Similarly, Li^+ ions are inserted into the respective two lattice sites during discharge leading to appearance of two cathodic current peaks. There is an increase in the size of voltammograms with an increase in sweep rates in all solutions. A clear separation of the two anodic peaks as well as the cathodic peaks is observed at all sweep rates studied in 5 M LiNO_3 electrolyte of pH 6.5 (Fig. 3 (C)). However, the peaks tend to merge at high scan rates in acidic as well as in alkaline electrolytes (Fig. 3(A), (B) and (D)). It is also observed that at a particular sweep rate, current increases with an increase of pH of the electrolyte. As voltammograms with clearly separated current peaks were obtained in 5 M LiNO_3 of pH 6.5 (Fig. 3(C)), the rest of the experiments were conducted in this solution. The effect of sweep rate was examined by plotting the peak currents of all four peaks against sweep rate (ν) and also against $\nu^{1/2}$. It was found that the peak current increases linearly with ν , but not with $\nu^{1/2}$. Similar observations are reported by Nakayama et al., recently [10]. It is known that if a redox process occurs by diffusion of species dissolved in the electrolyte, the peak current is directly proportional to $\nu^{1/2}$, and the peak potential separation, ΔE_p is equal to $0.06/n$ V, where n is the number of electrons [11]. On the other hand, if the redox species is bound to the electrode surface, the peak current should be proportional to ν , and ΔE_p is close to zero mV. In the present study, the redox species, namely, Mn^{3+} and Mn^{4+} are present in LiMn_2O_4 , which is coated on the current collector. Therefore, the peak current is proportional to ν as expected. The value of ΔE_p is also close to zero mV at low sweep rates. In neutral electrolyte (Fig. 3 (C)) at the sweep rate of 0.05 mV s^{-1} , for instance, the values of ΔE_p are 8 and 12 mV for the first and second pairs of redox peaks, respectively.

3.4. Charge-discharge cycling

The variation of potential of LiMn_2O_4 electrode during a typical charge-discharge cycling is shown in Fig. 4(A). Both the charge and discharge curves consist of two potential plateaus corresponding two stages of intercalation and de-intercalation as discussed for the appearance of two pairs of cyclic voltammetric peaks (Fig. 3). The lower potential plateau of the charging curve is attributed to the equilibrium between LiMn_2O_4 and $\text{Li}_{0.5}\text{Mn}_2\text{O}_4$; and the upper plateau to the equilibrium between $\text{Li}_{0.5}\text{Mn}_2\text{O}_4$ and $\lambda\text{-MnO}_2$, which accompany the deintercalation of Li^+ ions in aqueous electrolytes. The sharp increase of potential at about 1.1 V on the charging curve (Fig. 4(A)) is due to the onset of oxygen evolution reaction (OER). During the discharge step, potential decreases gradually from about 1.15 V to 0.7 V in two plateaus similar to the charging step. There is a sharp decrease of potential at 0.7 V indicating the end of discharge. The discharge capacity obtained at C/1.5 rate is about 73 mA h g^{-1} . Pei et al., studied electrochemical behavior of LiMn_2O_4 in Zn – LiMn_2O_4 cell consisting of aqueous 5 M LiNO_3 electrolyte and reported discharge capacity in the range of 70 –

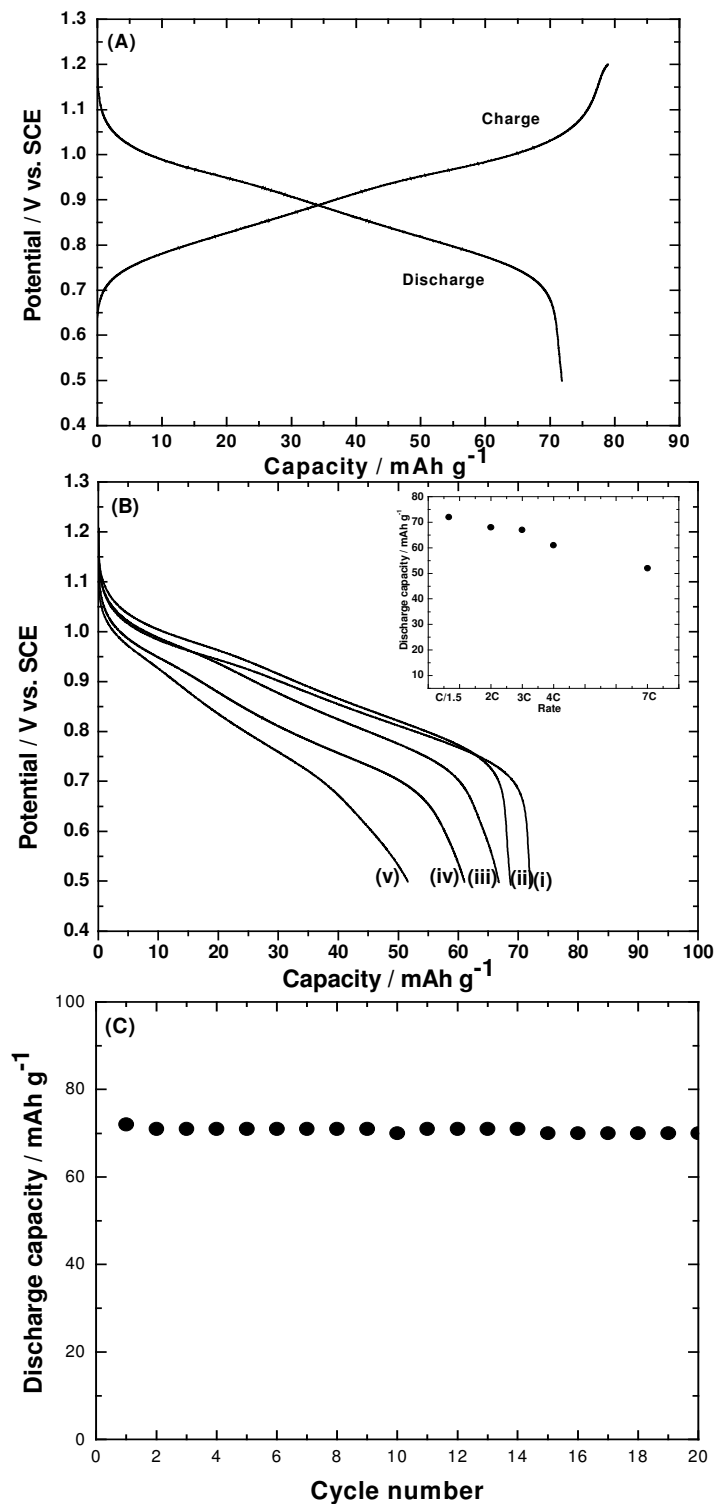


Figure 4. (A) Typical charge-discharge curves of LiMn_2O_4 electrode at C/1.5 rate, (B) discharge curves of LiMn_2O_4 electrode at C/1.5 (i), 2C (ii), 3C (iii), 4C (iv) and 7C (v) rates, and (C) variation of discharge capacity of LiMn_2O_4 electrode with cycle number at C/1.5 rate. Inset in (B) is variation of discharge capacity with rate of cycling.

80 mA h g⁻¹ [12], similar to the value obtained in the present study. Kohler et al., studied charge-discharge behavior of LiV₃O₈-LiNi_{0.81}Co_{0.19}O₂ cell in aqueous 1 M Li₂SO₄ electrolyte [13]. They obtained cell capacity values in the range of 20 - 40 mAh g⁻¹ range, which is only 15 – 30 % of the theoretical capacity. The reasons ascribed for low capacity included the cell voltage close to the electrolysis voltage of water, a significant voltage drop during the initial stages of charge-discharge cycling and sharp inclining/declining charge/discharge curves which cause a rapid reach of voltage to the limiting values. Although, the theoretical value of capacity of LiMn₂O₄ is about 130 mAh g⁻¹, which corresponds to the complete deintercalation/ intercalation of Li⁺, the charging capacity obtained is only about 73 mAh g⁻¹ in the present study also due to the above reasons. Although some of Li⁺ in LiMn₂O₄ is occupied by Na⁺ as an impurity as discussed in Section 3.2., it is likely that Na⁺ ions get deintercalated from the oxide into the electrolyte during the initial charging step. Once Na⁺ is transferred into the electrolyte, which is a concentrated solution of Li⁺ salt (5 M LiNO₃), its concentration becomes very low and it cannot get intercalated into the lattice of LiMn₂O₄ during the subsequent discharge process. Therefore, the small amount of Na does not have significant influence on electrochemical behavior of the compound.

A LiMn₂O₄ electrode was subjected to charge-discharge cycling at various rates. The discharge curves are shown in Fig. 4(B), and the discharge capacity is shown as a function of rate in inset of Fig. 4(B). It is seen that the two plateaus are clearly present at high rates of discharge (Fig. 4(B)). It is interesting to note that the electrode can be cycled at a rate as high as 7C in the aqueous electrolyte. There is a slight decrease in capacity from about 73 mAh g⁻¹ at C/1.5 rate to about 50 mAh g⁻¹ at 7C rate. This means, the electrode can be discharged in less than 10 min and a discharge capacity which is about 40 % of the theoretical capacity can be realized. It may be noted that LiMn₂O₄ electrode in non-aqueous electrolytes cannot be cycled at such high rates, and fast charging of the present Li-ion batteries is essential if they are intended for use in electric vehicles. The higher rate of charge-discharge cycling in the aqueous medium suggests a faster rate of intercalation/deintercalation process, which is perhaps assisted by greater conductivity when compared with the rate capability of LiMn₂O₄ in the non-aqueous media and also due to sub-micron size of the particles. A LiMn₂O₄ electrode was subjected to repeated charge-discharge cycling at C/1.5 rate and the discharge capacity is found to be stable at about 70 mAh g⁻¹ (Fig. 4(C)).

3.5. AC impedance studies of LiMn₂O₄

Intercalation/deintercalation of Li⁺ in LiMn₂O₄ accompanies the Mn³⁺/Mn⁴⁺ redox process in solid state within the oxide. Although various aspects of LiMn₂O₄ related to structural studies are widely reported [14], electrochemical studies pertaining to properties of the redox reaction are scarce. LiMn₂O₄ prepared in the present study was subjected to ac impedance studies at different temperatures and various states-of-charge (SOC). From these data exchange current, transfer coefficient (α) and activation energy (E_a) for the Mn³⁺/Mn⁴⁺ redox reaction were evaluated as detailed below. Similar studies were earlier reported for a commercial non-aqueous Li-ion cell [15]. Nyquist impedance plots are shown in Fig. 5 typically at SOC \approx 0.5 for various temperatures, and in Fig. 6 at 20 °C for various

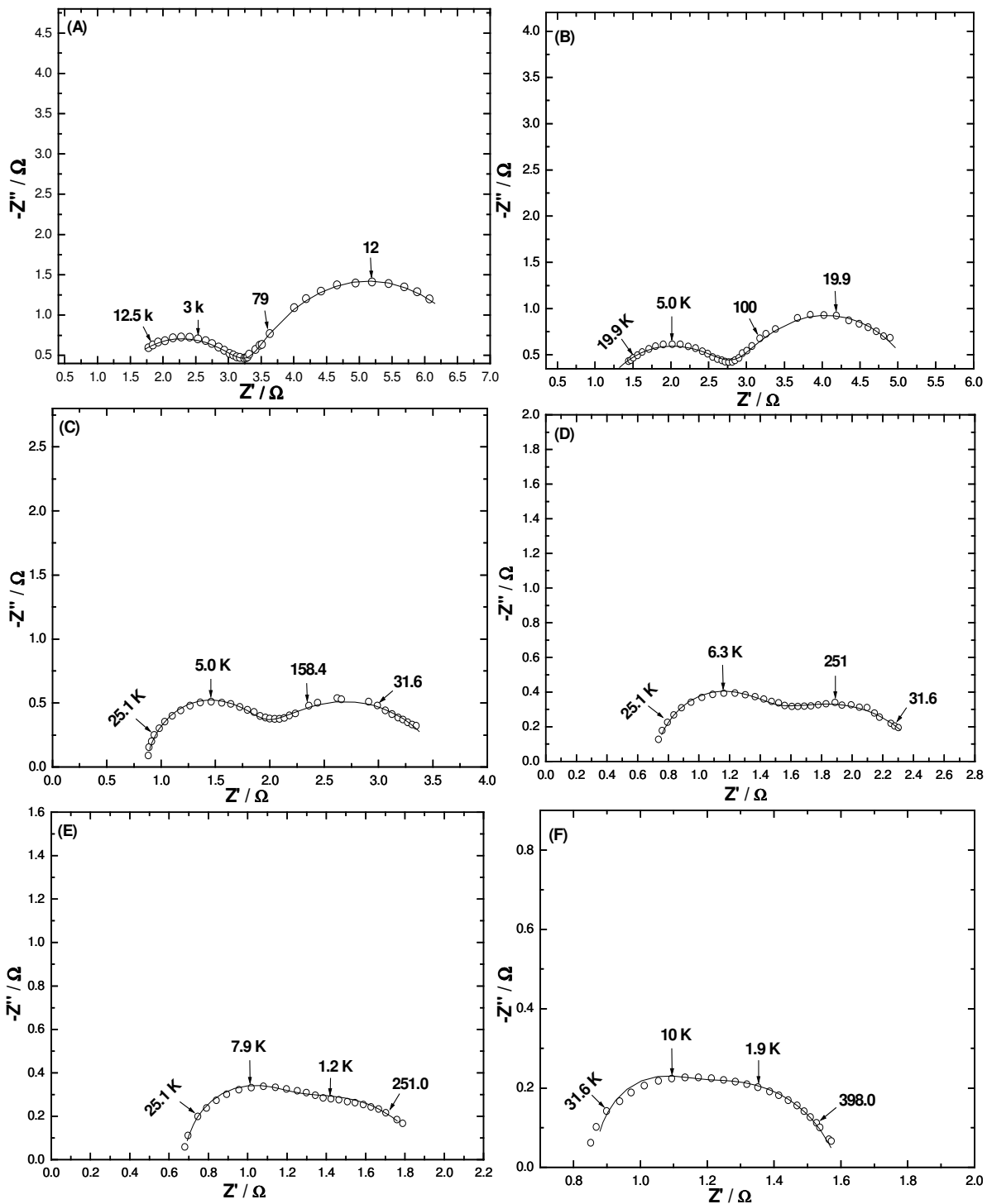


Figure 5. Nyquist impedance spectra of the LiMn_2O_4 electrode at SOC~ 0.5 at different temperatures (A) -5, (B) 0, (C) 10, (D) 20 , (E) 30, and (F) 40 °C. Experimental data are shown as open circles and theoretical data obtained from fitting are shown as curves. Frequency of some data points are given in Hz.

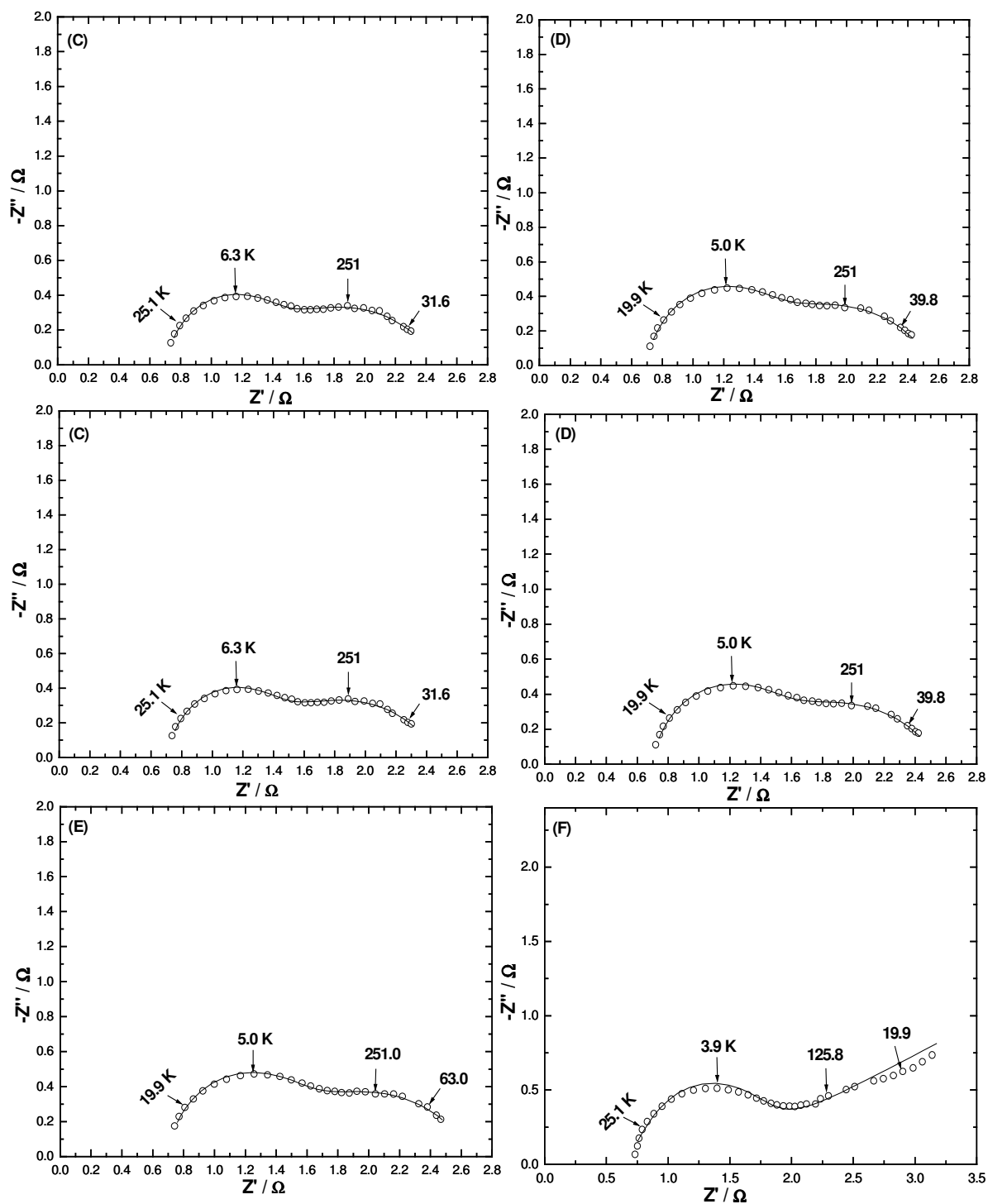


Figure 6. Nyquist impedance spectra of the LiMn_2O_4 electrode at temperature 20°C at different SOC values (A) 1.0, (B) 0.78, (C) 0.56, (D) 0.35, (E) 0.13, (F) 0.0. Experimental data are shown as open circles and theoretical data obtained from fitting are shown as curves. Frequency of some data points are given in Hz.

SOC values. At all temperatures and SOC values, a high frequency intercept, a small semicircle in the middle frequency range and a larger semicircle in the low frequency range are present. The impedance parameters were evaluated by fitting the data to an equivalent circuit using a non-linear least squares (NLLS) fitting program [16]. The suitable equivalent circuit, which was found to fit the impedance data, is shown in Fig. 7. Resistance R_{Ω} represents the ohmic resistance, which includes the resistance

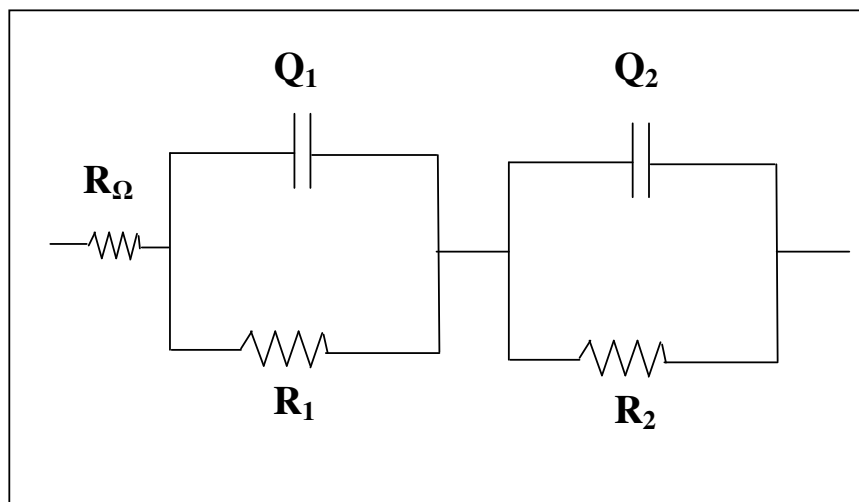


Figure 7. Equivalent circuit used for NLLS-fitting of the experimental impedance data (See text for symbols).

of the electrolyte, current collectors, electrical leads etc. The two semicircles (Figs. 5 and 6) of each Nyquist plot are due to two pairs of parallel resistance and capacitances [17]. Because the semicircles are depressed with their centers below the real axis, capacitors are replaced by constant phase element (CPE, Q) in Fig. 7 [18]. Accordingly, R_1 and Q_1 are resistance and CPE, respectively; corresponding to the high frequency semicircle, and R_2 and Q_2 are resistance and CPE, respectively, corresponding to the low frequency semicircle. Constant phase element (Q) is mathematically defined in admittance from as [18,19],

$$Q = Q^0 (j\omega)^{-n} \quad (1)$$

where Q^0 is an adjustable parameter, ω is angular frequency and n is a constant. If $n = 1$, the CPE represents a capacitance (C) with $Q^0 = C$. Similar to the data of the LiMn_2O_4 electrode obtained in the present study, impedance of LiCoO_2 in non-aqueous electrolytes was shown to consist of two semicircles [20]. It was concluded that the formation of a surface layer on the LiCoO_2 was responsible for the high frequency semicircle and the kinetics of redox process of transition metal ion accompanying the intercalation/deintercalation of Li^+ in the electrode for the low frequency semicircle. Accordingly R_1 is resistance of surface film on LiMn_2O_4 and Q_1 is CPE corresponding to capacitance of the surface film. The impedance parameters, R_2 and Q_2 are resistance and CPE, respectively,

corresponding to the electrochemical $\text{Mn}^{3+}/\text{Mn}^{4+}$ redox process and double-layer capacitance. The impedance parameters were obtained by fitting the data (Figs. 5 and 6) to the equivalent circuit (Fig. 7). The resistance R_2 is equivalent to charge-transfer resistance ($R_{ct} = R_2$) of the electrochemical process.



In general R_{ct} is approximately related to the reaction kinetics from Butler-Volmer equation for charge-transfer controlled reaction (Eq.3) [21].

$$R_{ct} = R T / (F I_0) \quad (3)$$

where R is gas constant, T absolute temperature, F faraday constant and I_0 exchange current of the reaction. The values of I_0 of the Reaction (2) in LiMn_2O_4 were calculated, and its variation with SOC, typically at 20°C , is shown in Fig. 8. The value of I_0 increases with SOC and also with temperature. These features indicate that high temperatures and high SOC values favor the kinetics of Reaction (2).

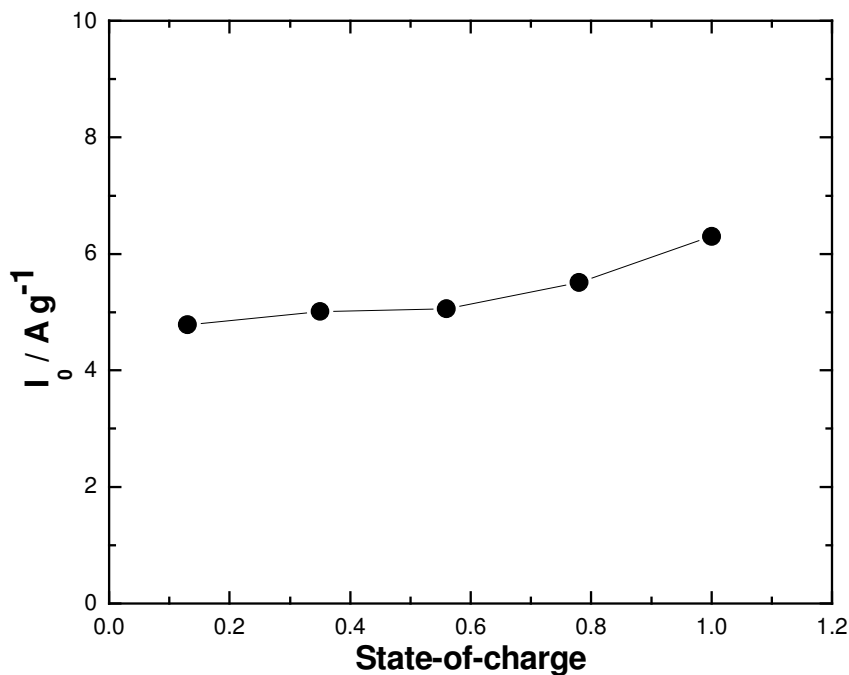


Figure 8. Variation of exchange current density (I_0) with state-of-charge of LiMn_2O_4 electrode at 20°C

The relationship between I_0 and concentrations (C) of Mn^{4+} and Mn^{3+} in $\text{Li}_x\text{Mn}_2\text{O}_4$ is given in Eq. (4) [22]. In $\text{Li}_x\text{Mn}_2\text{O}_4$, $x \approx 1$ when the electrode attains $\text{SOC} \approx 0$. At this state half of the manganese present is in 3+ and the other half in 4+ oxidation states. When the electrode reaches SOC

≈ 1 , the value of x is close to zero and the whole of manganese reaches the oxidation state of 4+. C_{Mn3+} refers to the amount of Mn^{3+} ions that can undergo oxidation and C_{Mn4+} to the amount of Mn^{4+} ions that can be formed from the oxidation of Mn^{3+} ions in the solid $Li_xMn_2O_4$.

$$I_o = F k_s C_{Mn3+}^\alpha C_{Mn4+}^{(1-\alpha)} \quad (4)$$

where k_s is the standard rate constant and α the transfer coefficient [22]. The discharge capacity of the electrode is governed by the amount of Mn^{4+} that can undergo reduction to Mn^{3+} . Thus, the SOC is defined as the ratio of the amount (C_{Mn4+}) of Mn^{4+} available for reduction at the SOC to the maximum amount ($C_{Mn4+(m)}$) of Mn^{4+} that can be reduced in the electrode. Thus,

$$S = C_{Mn4+} / C_{Mn4+(m)} \quad (5)$$

where SOC is abbreviated as S. Therefore,

$$C_{Mn4+}^{(1-\alpha)} = k_1 S^{(1-\alpha)} \quad (6)$$

where $k_1 (= C_{Mn4+(m)}^{(1-\alpha)})$ is a constant. Also,

$$C_{Mn3+} = C_{Mn4+(m)} - C_{Mn4+} \quad (7)$$

From Eq. (7), Eq. (5) can be rewritten as:

$$S = (C_{Mn4+(m)} - C_{Mn3+}) / C_{Mn4+(m)} \quad (8)$$

Therefore,

$$C_{Mn3+} / C_{Mn4+(m)} = (1 - S) \quad (9)$$

$$C_{Mn3+}^\alpha = k_2 (1-S)^\alpha \quad (10)$$

where $k_2 (= C_{Mn4+(m)}^\alpha)$ is a constant.

From Eqs. (6) and (10), we can rewrite Eq. (4) as:

$$I_o = F k_s k_1 k_2 S ((1 - S) / S)^\alpha \quad (11)$$

Using Eq. (11), we can write Eq. (3) as in Eq. (12).

$$R_{ct} = R T / (F^2 k_s k_1 k_2 S ((1 - S) / S)^\alpha) \quad (12)$$

The standard rate constant (k_s) depends on T, and the relationship follows Arrhenius equation:

$$k_s = A_o \exp(-E_a / R T) \quad (13)$$

where E_a is activation energy and A_o a constant. From Eq. (13), Eq. (12) becomes:

$$R_{ct} = \frac{k T \exp(E_a / R T)}{S ((1 - S) / S)^\alpha} \quad (14)$$

where k ($= R / (F^2 A_o k_1 k_2)$) is a constant, which is independent of T and SOC. Since T and S are independent of each other, we can rewrite Eq. (14) as in Eq. (15),

$$\ln (R_{ct} / T) = \ln k + (E_a / (R T)) - \ln S - \alpha \ln ((1 - S) / S) \quad (15)$$

On differentiation, we get at constant S ,

$$\frac{d \ln(R_{ct} / T)}{d (1/T)} = E_a / R \quad (16)$$

Eq. (14) can also be rewritten as:

$$\ln (R_{ct} S) = \ln (k T) + (E_a / (RT)) - \alpha \ln ((1 - S) / S) \quad (17)$$

On differentiation, we get at constant T ,

$$\frac{d \ln (R_{ct} S)}{d \ln ((1 - S) / S)} = -\alpha \quad (18)$$

Thus, it is possible to evaluate apparent activation energy (E_a) and apparent transfer coefficient (α) for the Mn^{4+} / Mn^{3+} redox process in $LiMn_2O_4$.

The variation of $\ln (R_{ct} / T)$ with $10^3/T$ for the $LiMn_2O_4$ electrode is shown in Fig. 9, typically from the data measured at SOC ≈ 0.5 . It is seen that the plot is linear as expected from Eq. (16). Similar linear plots were drawn from the data measured at other SOC values also. The values of E_a obtained from Fig. 9 for SOC ≈ 0.5 value is 0.32 eV. The values of E_a calculated are in the range from 0.30 to 0.35 eV for the whole range of SOC, and there is no regular trend observed for variation of E_a with SOC. Because there are two pairs of redox peaks in cyclic voltammograms (Fig. 3) and also two plateau regions during charge – discharge cycling (Fig. 4(A)), we anticipated two different ranges of E_a values, one range corresponding to the SOC range from 0 to 0.5 and the other to the SOC range from 0.5 to 1.0. However, we did not observe such clear demarcation of E_a values between lower and upper ranges of SOC. The variation of $\ln (R_{ct} S)$ with $\ln ((1 - S) / S)$ for the $LiMn_2O_4$ electrode is shown in Fig. 10, typically from the data measured at 20 °C. The variation is linear as expected from Eq. (18). The value of α calculated from the slope of the plot (Fig. 10) is 0.51. The range of α values calculated

from the data measured at various temperatures is 0.44 - 0.55. As the value of α expected for a reversible electron transfer reaction is 0.5, the values obtained from the present study suggest that the Mn^{3+}/Mn^{4+} redox process is reversible.

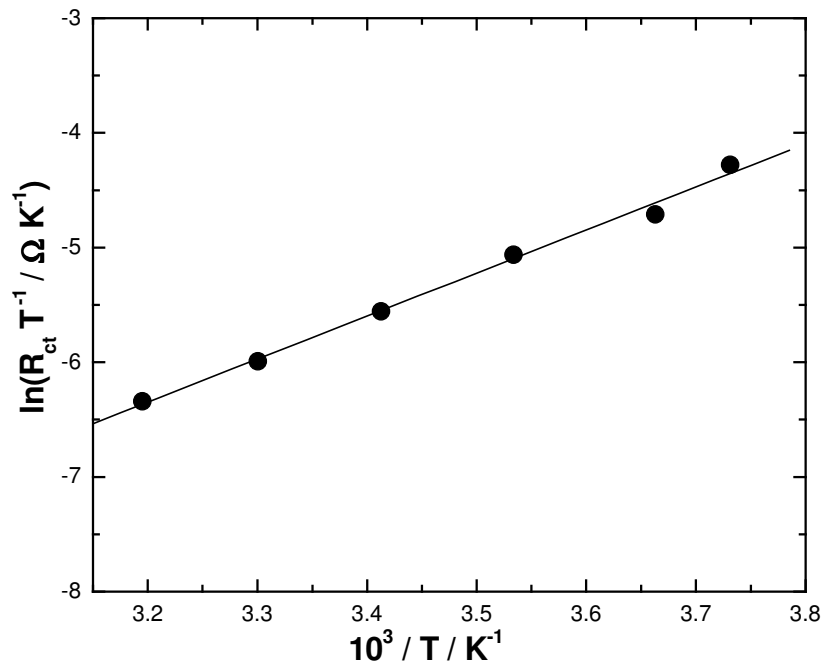


Figure 9. Variaton of $\ln (R_{ct} / T)$ against inverse of temperature (T) for state-of-charge ≈ 0.5 .

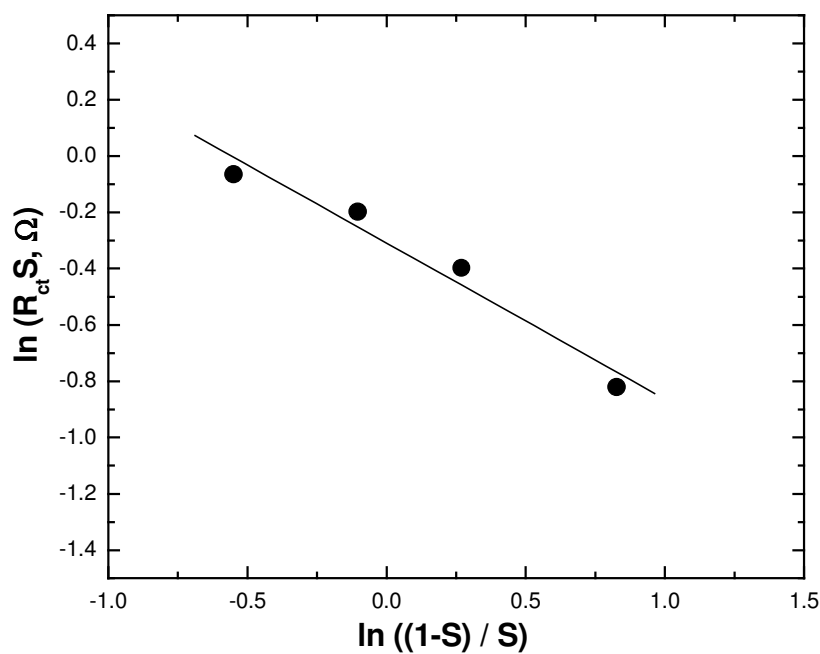


Figure 10. Variation of $\ln (R_{ct} S)$ with $\ln ((1-S) / S)$ at 20 °C.

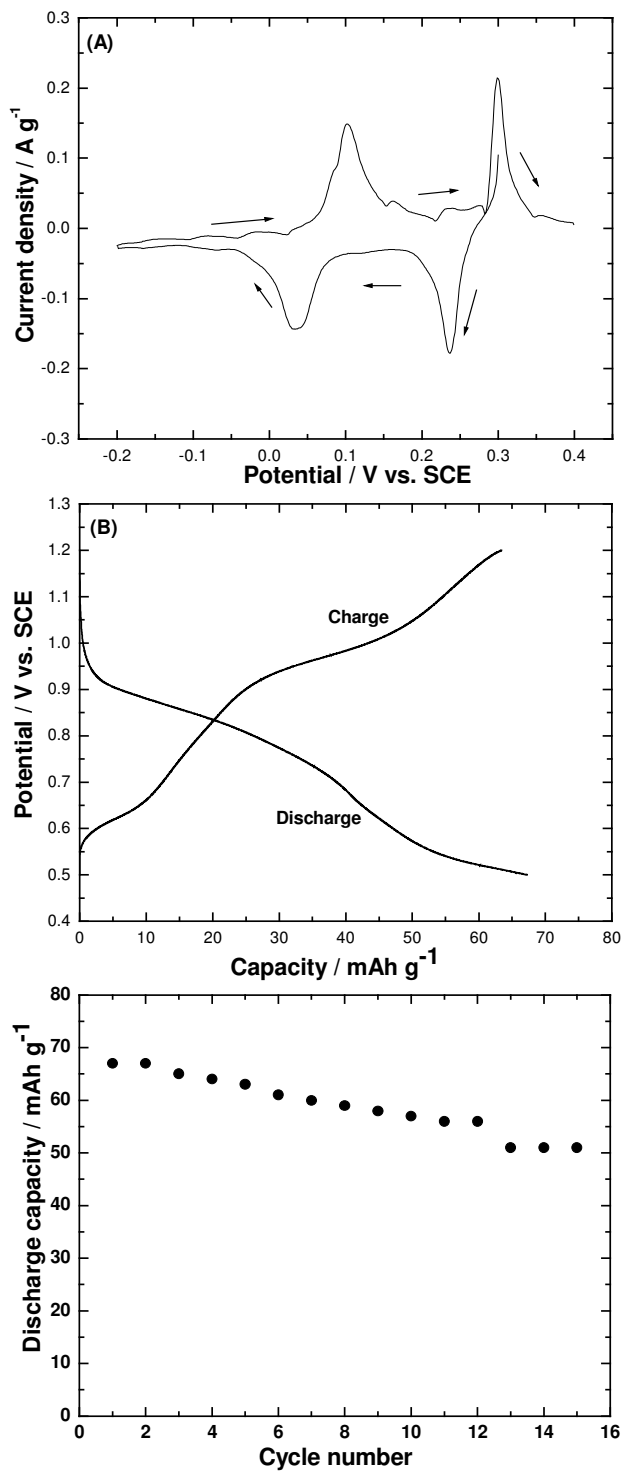


Figure 11. (A) Cyclic voltammogram of V_2O_5 in 5 M $LiNO_3$ aqueous electrolyte with scan rate 0.05 mV s^{-1} , (B) charge-discharge curves of the $V_2O_5 - LiMn_2O_4$ cell at 2C rate, and (C) cycling performance of the $V_2O_5//LiMn_2O_4$ cell at 2C rate.

3.6. V_2O_5 - $LiMn_2O_4$ cell studies

For the purpose of demonstration of a complete reversible cell in an aqueous electrolyte employing sub micron size $LiMn_2O_4$ particles prepared, V_2O_5 electrode was used as the negative electrode. A typical cyclic voltammogram of V_2O_5 in 5 M $LiNO_3$ is shown in Fig. 11(A). Two pairs of current peaks are observed in the potential range between -0.20 and 0.40 V. This range is negative to the range of potentials of current peaks observed for $LiMn_2O_4$ (Fig. 2). The two pairs of current peaks obtained for V_2O_5 are similar to the reported observations in non-aqueous electrolytes [23], thus suggesting the intercalation/deintercalation of Li^+ in V_2O_5 in aqueous electrolytes also [4]. A V_2O_5 - $LiMn_2O_4$ cell was constructed in 5 M $LiNO_3$ and subjected to charge-discharge cycling. Typical charge-discharge curves are presented in Fig. 11(B). The open-circuit voltage of the V_2O_5 - $LiMn_2O_4$ cell was 0.55 V and it was charged galvanostatically at 2C rate till the cell voltage reached 1.20 V. Subsequently, it was discharged down to 0.50 V. A couple of voltage plateaus are clearly observed on both the charge and discharge curves. A discharge capacity of about 70 mAh g^{-1} of $LiMn_2O_4$ is obtained during the initial charge-discharge cycle. However, there is a decrease in discharge capacity on repeated charge-discharge cycling as shown in Fig. 11(C), which is in contrast to the stable discharge capacity of $LiMn_2O_4$ shown in Fig. 4(C). The instability in discharge capacity of the V_2O_5 - $LiMn_2O_4$ cell is attributed to changes in crystallographic structure of V_2O_5 on repeated charge-discharge cycling.

4. CONCLUSIONS

Spinel $LiMn_2O_4$ was synthesized from microemulsion route and particles of size less than 200 nm were obtained [24]. $LiMn_2O_4$ electrode exhibited two pairs of reversible redox peaks and accordingly separate potential plateau are observed during charge-discharge cycling in 5 M $LiNO_3$ aqueous electrolyte. The electrodes made using sub micron size particles of $LiMn_2O_4$ were found to possess high rate capability in the aqueous electrolyte. Electrochemical impedance data measured at various temperatures and various state-of-charge (SOC) values were analyzed by a non-linear least squares fit procedure using an appropriate electrical equivalent circuit, and charge-transfer resistance (R_{ct}) of the redox process was evaluated. The parameters, exchange current, activation energy and transfer coefficient of the Mn^{3+}/Mn^{4+} process were calculated from variations of R_{ct} with temperature and SOC. A typical full cell employing $LiMn_2O_4$ as the positive electrode and V_2O_5 as the negative electrode was assembled and characterized by charge-discharge cycling in 5 M $LiNO_3$ aqueous electrolyte.

References

1. G. A. Nazri, and G. Pistoia, '*Lithium Batteries: Science and Technology*', Kluwer Academic Publishers, Boston, (2004) p.1
2. G. Pistoia, '*Lithium Batteries*'. Elsevier, Amsterdam, 1994) p.1
3. D. Linden, and T. B. Reddy, '*Handbook of Batteries*' McGraw-Hill Publishers, New York (2002) p 35.1

4. W. Li, J. R. Dahn, and D. S. Wainwright, *Science*, 264 (1994) 1115
5. P. Ragupathy, N. Munichandraiah, and H. N. Vasan, (2007) to be communicated.
6. B. L. Cushing, V. L. Kolesnichenko, and C. J. O'connor, *Chem. Rev.*, 104 (2004) 3893
7. Y. Xia, and M. Yoshio, *J. Electrochem. Soc.*, 143 (1996) 825
8. N. Cvjeticanin, I. Stojkovic, M. Mitric, and S. Mentus, *J. Power Sources*, 174 (2007) 1117
9. P. Shen, D. Jia, Y. Huang, L. Liu, and Z. Guo, *J. Power Sources*, 158 (2006) 608
10. N. Nakayama, T. Nozawa, Y. Iriyama, T. Abe, Z. Ogumi, and K. Kikuchi, *J. Power Sources*, 174 (2007) 695
11. R. Greef, R. Peat, L. M. Pletcher, and J. Robinson, '*Instrumental Methods in Electrochemistry*' John Willey & Sons, New York (1985) p.1
12. W. Pei, Y. Hui, and Y. Huaquan, *J. Power Sources*, 63 (1996) 275
13. J. Kohler, H. Makihara, H. Uegatio, H. Inoue, and M. Toki, *Electrochim. Acta*, 46 (2000) 59
14. M. S. Wittingham, *Chem. Rev.*, 104 (2004) 4271
- 15.
16. P. Suresh, A. K. Shukla and N. Munichandraiah, *J. Appl. Electrochem.*, 32 (2002) 267
17. S. Rodrigues, N. Munichandraiah, and A.K. Shukla, *J. Solid State Electrochem.*, 3 (1999) 397
18. B. A. Boukamp, '*Equivalent Circuit: Users Manual*' University of Twente, The Netherlands, (1989) p.1
19. J. R. Macdonald, '*Impedance Spectroscopy*' John Willey & Sons, New York (1987) p.1
20. M.G.S.R. Thomas, P.G. Bruce, and J.B. Goodenough, *J. Electrochem. Soc.*, 132 (1985) 1521
21. A. J. Bard, and L. R. Faulkner in '*Electrochemical Methods*', John Willey & Sons, New York (1980) p. 105
22. P. Delahay, '*Double Layer and Electrode Kinetics*', Interscience Publishers, New York (1965) p. 153
23. A. Shimuzu, T. Tsumura, and M. Inagaki, *Solid State Ionics*, 63 (1993) 479
24. Nupur Nikkan Sinha, and N. Munichandraiah, *J. Solid State Electrochem.* (2008) in press.